IEEE Access
Multidisciplinary | Rapid Review | Open Access Journal

Received January 21, 2019, accepted February 7, 2019, date of publication February 18, 2019, date of current version March 5, 2019.

Digital Object Identifier 10.1109/ACCESS.2019.2899990

Deep Neural Networks for Channel Estimation in Underwater Acoustic OFDM Systems

RONGKUN JIANG[1], XUETIAN WANG[1], SHAN CAO[2], JIAFEI ZHAO[1], AND XIAORAN LI[1]
[1]School of Information and Electronics, Beijing Institute of Technology, Beijing 100081, China
[2]Department of Communication and Information Engineering, Shanghai University, Shanghai 200444, China

Corresponding author: Xiaoran Li (xiaoran.li@bit.edu.cn)

This work was supported by the National Natural Science Foundation of China under Grant 61801027 and China Postdoctoral Science Foundation under Grant 2018M631356.

ABSTRACT Orthogonal frequency division multiplexing (OFDM) provides a promising modulation technique for underwater acoustic (UWA) communication systems. It is indispensable to obtain channel state information for channel estimation to handle the various channel distortions and interferences. However, the conventional channel estimation methods such as least square (LS), minimum mean square error (MMSE) and back propagation neural network (BPNN) cannot be directly applied to UWA-OFDM systems, since complicated multipath channels may cause a serious decline in performance estimation. To address the issue, two types of channel estimators based on deep neural networks (DNNs) are proposed with a novel training strategy in this paper. The proposed DNN models are trained with the received pilot symbols and the correct channel impulse responses in the training process, and then the estimated channel impulse responses are offered by the proposed DNN models in the working process. The experimental results demonstrate that the proposed methods outperform LS, BPNN algorithms and are comparable to the MMSE algorithm in respect to bit error rate and normalized mean square error. Meanwhile, there is no requirement of prior statistics information about channel autocorrelation matrix and noise variance for our proposals to estimate channels in UWA-OFDM systems, which is superior to the MMSE algorithm. Our proposed DNN models achieve better performance using 16QAM than 32QAM, 64QAM, furthermore, the specified DNN architectures help improve real-time performance by saving runtime and storage resources for online UWA communications.

INDEX TERMS Deep neural networks, OFDM systems, channel estimation, underwater acoustic communication.

I. INTRODUCTION

Underwater acoustic (UWA) channels are usually regarded as one of the most difficult communication mediums [1]–[3]. Compared to general wireless communication scenarios, UWA channels suffer from a variety of environmental factors, including temperature, salinity, pressure, limited bandwidth, multipath effect, Doppler shift, transmission loss, ocean noise and so on [4]–[7]. These complicated UWA environment places higher requirements and greater challenges to achieve high-efficiency and reliable transmissions for wireless communication. More recently, the orthogonal frequency division multiplexing (OFDM) technique has been adopted to UWA communications, due to its excellent performance in resisting inter symbol interference (ISI) and reducing multipath fading effect [8]–[10]. As a multicarrier system, OFDM divides the channel bandwidth into a large number of orthogonal narrowband subcarriers, such that each individual subcarrier which occupies only a small bandwidth can be modulated with a conventional modulation scheme at a low data rate, maintaining the total data rates equal to a single carrier system with the same bandwidth [11]. This feature guarantees OFDM systems with high-speed transmission and high spectrum efficiency for wireless communication over UWA multipath channels.

Channel estimation is critical to the performance of UWA-OFDM systems [12]. Since the transmission signal is generally distorted by the channel characteristics when through multipath channels, the channel impulse response (CIR) must be estimated to recover the transmitted signal coherently at the receiver. To this end, some pilot symbols are usually sent together with the data subcarriers to obtain the CIR for channel estimation, where the pilot symbols are also priori known to the receiver. With the help of these pilot

The associate editor coordinating the review of this manuscript and approving it for publication was Yangming Li.

symbols, estimation techniques can then be utilized to evaluate the significant information of CIR for UWA-OFDM systems, such as least squares (LS) algorithm, minimum mean square error (MMSE) algorithm [13], [14].

A. RELATED WORK

In recent years, there have been a growing interest in artificial neural network (ANN), for its strong ability to learn from the environments in supervised as well as unsupervised ways, mimicking the human brain with numerous interconnected neurons [15]. This advantage makes it highly suitable for solving complex nonlinear problems, including image recognition [16], signal processing [17], computer vision [18], robotics [19]–[22] and so on. In particular, many types of neural networks have been successfully applied to the problem of channel estimation in wireless communications. In [23]–[25], a type of radial basis function (RBF) neural network was proposed for channel estimation in pilot symbol aided OFDM systems, the structure of which was designed by the pilot pattern to effectively restore the channel response. Reference [26] developed an ANN channel estimation technique for OFDM systems without assistance of pilot symbols over Rayleigh fading channels, increasing the bandwidth efficiency compared to pilot-based estimation techniques. For multiple input multiple output-orthogonal frequency division multiplexing (MIMO-OFDM) systems, ANN-based channel estimators were presented to estimate channel effect using comb-type pilot arrangement in [27] and trained continuously by feedback symbols over mobile communications channels in [28]. Among many network models, one of the most commonly used is back propagation neural network (BPNN) with three layers of neurons, generally proposed to estimate the channel characteristics of OFDM systems [29]–[32]. In [33]–[36], BPNNs were expanded into space time coded MIMO-OFDM systems and orthogonal frequency division multiplexing-interleave division multiple access (OFDM-IDMA) systems for estimating the channel coefficients. Furthermore, [37] combined the BPNN with genetic algorithm to improve the estimation performance and convergence rate, which is usually used to search for reliable solutions to optimization problems.

However, if the aforementioned neural networks are directly applied to channel estimation in complex communication scenarios for UWA-OFDM systems, it may cause a serious decline in estimation performance since underwater acoustic environment is far more complicated in the reality whereas these networks are sensitive to the environmental variations. To address the issue, it seems that deep neural network (DNN) may be a promising choice. Comprising of much more layers and neurons, the DNN models are flexible with a large number of parameters and have stronger generalization ability to deal with the UWA environment than traditional BPNN models.

Although DNN has gained great attention in the fields of artificial intelligence (AI) and machine learning for a long time [38]–[41], only a limited number of references have investigated the DNN applications for wireless communications in recent years. Reference [42] and [43] proposed DNN approaches for fingerprinting-based indoor localization with commodity 5G WiFi networks. Reference [44] introduced a new signal detection scheme based on DNN model for OFDM systems. Reference [45] proposed an efficient online CSI prediction scheme with DNN for 5G wireless communication systems. Reference [46] and [47] investigated the use of DNN models in modulation classification for communication systems. Reference [48] adopted the autoencoder architecture of DNN to solve the problem of high peak to average power ratio (PAPR) in OFDM systems. In [49], a new DNN architecture named Cascade-Net was considered for OFDM symbol detection in combating large Doppler shift. Reference [50] developed novel DNN based architectures and methodologies for OFDM receivers under the constraint of one-bit complex quantization. In [51], a model-driven approach combining DNN with the expert knowledge was proposed to recover the transmitted data in OFDM systems with linear and nonlinear distortions. Especially for UWA communications, in [52], a five-layer DNN with neurons of 256, 500, 250, 120, 16 in each layer was trained as a black box with the offline simulated data for channel estimation and symbol detection in OFDM systems. [53] proposed a DNN model for joint channel equalization and decoding, in which the numbers of neurons in six layers were 16, 256, 128, 64, 32, 8 respectively. In [54], a DNN based receiver with neurons of 1024, 1500, 600, 128, and 32 for the five layers was presented to recover the transmitted signal directly after sufficient training.

These previous papers provide a feasible guidance for the application of DNN to complex UWA communications, but the obstacles of these DNN models in [52]–[54] are that a massive number of storage resources are needed to preserve the network parameters, and a high latency of running time will occur during the application process. Different from these DNN models, we attempt to design a properly sized neural network architecture to save storage resources and running time while satisfying the desired performance requirements for channel estimation in UWA-OFDM systems.

B. OUR CONTRIBUTION

In this paper, two specific architectures of DNN models are proposed for channel estimation to mitigate the impact of environmental variations in UWA-OFDM systems, modeling with various tapped UWA multipath channels for different scenarios. Our proposed DNN-based estimators are trained by training samples to learn the characteristics of UWA multipath channels, which suffer from various nonlinear distortions and interferences. Experiments are conducted to investigate the performance of channel estimation and the impact of different modulation schemes with 16QAM, 32QAM, and 64QAM for the considered LS, MMSE, BPNN, and the proposed DNN methods in terms of bit error rate (BER) and normalized mean square error (NMSE) versus signal to noise ratio (SNR) criteria. Moreover, running time

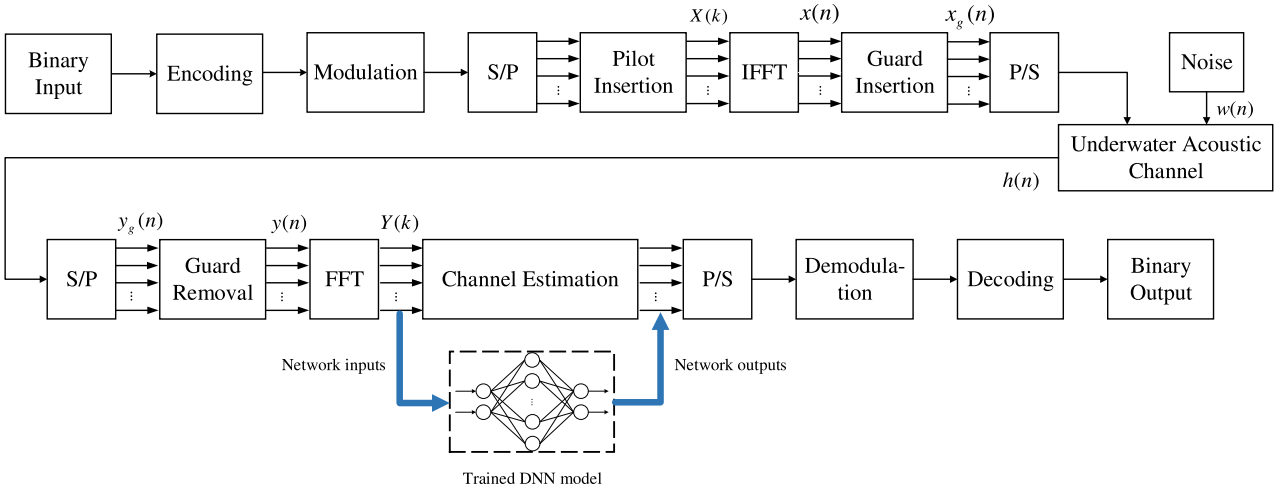

FIGURE 1. Block diagram of UWA-OFDM system model. The main idea of the OFDM technique is that the serial signal is converted into multiple parallel signal by IFFT at the transmitter (upper part of the diagram) and the parallel signal is restored to serial signal by FFT at the receiver (lower part of the diagram). In UWA-OFDM sytems, pilot symbols are embedded into the transmitted signal to help for channel estimation, both in traditional methods and our proposed DNN methods (shown as the blue data streams).

and storage resources are compared to analyse the real-time performance for neural network based methods.

The primary contribution of our work can be summarized as follows:

1) We introduce the DNN solutions to solve the problem of channel estimation in UWA-OFDM systems, where the BELLHOP ray model is applied to simulate the UWA communication environment for increasing the reliability and accuracy of experiments.
2) We propose two DNN models with different architectures employing a novel training strategy for channel estimation.
3) We perform extensive experiments on the proposed DNN models to compare and analyse the results with conventional LS, MMSE, and BPNN channel estimation methods.

Accordingly, experimental results demonstrate that our proposed DNN methods outperform LS, BPNN algorithms with regard to BER and NMSE, meanwhile they are superior to MMSE algorithm without requiring prior statistics information about UWA multipath channels. Moreover, it is discovered that different modulation schemes affect the estimation performance of UWA-OFDM systems, in which the DNN-based estimators with 16QAM offer better performance than those with 32QAM and 64QAM. Furthermore, compared with the DNN models in [52]–[54], the proposed DNN methods can save running time and storage resources to improve real-time performance for online UWA communications.

The remainder of this paper is organized as follows. Section II describes the UWA-OFDM system model and the problem of channel estimation. Section III presents the proposed methods based on DNN for channel estimation, including the basic knowledge, network architectures, and network training. Experimental results and analyses are given in Section IV. Finally, Section V concludes the paper.

II. PROBLEM DESCRIPTION

A. UWA-OFDM SYSTEM MODEL

A schematic diagram of the UWA-OFDM system model [55]–[58] is illuminated in Fig. 1.

Suppose that the binary data sequence is firstly encoded and mapped with quadrature amplitude modulation (QAM) modulation schemes. The modulated signal is converted from serial to parallel ones, and the pilot tones are inserted to estimate the CIR of the channel model. In the UWA-OFDM system, the parallel data are transformed by inverse fast Fourier transform (IFFT) with N orthogonal narrowband subcarriers. The time domain signal $x(n)$ is obtained from the frequency domain signals $X(k)$ as follows:

$$\begin{aligned} x(n) &= \mathbf{IFFT}\{X(k)\} \\ &= \frac{1}{N}\sum_{k=0}^{N-1} X(k)e^{j\frac{2\pi}{N}nk}, \quad n = 0, 1, \ldots, N-1 \end{aligned} \tag{1}$$

After IFFT, the N parallel subcarriers are converted to a serial bitstream and the cyclic prefix samples are inserted as guard intervals to alleviate the ISI. So the time-domain transmitted signal including cyclic prefix can be represented as follows:

$$x_g(n) = \begin{cases} x(N+n), & n = -N_g, \ -N_g+1, \ldots, -1 \\ x(n), & n = 0, 1, \ldots, N-1 \end{cases} \tag{2}$$

where N_g is the length of cyclic prefix samples. It means that the last N_g samples of $x(n)$ are duplicated as cyclic prefix and inserted to the beginning of this symbol, resulting the signal $x_g(n)$ with length of $N + N_g$.

After through the underwater acoustic channel, the received signal $y_g(n)$ is given by:

$$y_g(n) = x_g(n) \otimes h(n) + w(n), \ -N_g \le n \le N-1 \tag{3}$$

where the operator $\otimes$ corresponds to the circular convolution and $w(n)$ is the additive white Gaussian noise (AWGN) with zero-mean. $h(n)$ is the channel impulse response that can be represented as follows:

$$h(n) = \sum_{i=0}^{r-1} h_i \delta\left(n - \tau_i\right) \tag{4}$$

where δ is impulse response, r is the number of multipaths, h_i and τ_i are the discrete complex gain and time delay of the i-th tap.

In the receiver, the received signal is split into parallel subcarriers and the cyclic prefix is removed out. Then the time-domain signal $y(n)$ is transformed to frequency-domain signal $Y(k)$ by fast Fourier transform (FFT) operations as follows:

$$\begin{aligned} Y(k) &= \mathbf{FFT}\left\{y(n)\right\} \\ &= \frac{1}{N}\sum_{n=0}^{N-1} y(n) e^{-j\frac{2\pi}{N}nk}, \quad k = 0, 1, \ldots, N-1 \end{aligned} \tag{5}$$

thus under the assumption that the ISI is completely eliminated, the received signal can be formulated as:

$$Y(k) = X(k)H(k) + W(k), \quad k = 0, 1, \ldots, N-1 \tag{6}$$

where $H(k)$, $W(k)$ are the Fourier transform of $h(n)$ and $w(n)$, respectively. It is noted that the relationship between the transmitted signal and received signal for a UWA channel can be clearly expressed by means of $H(k)$ and $W(k)$ in the frequency-domain.

The compensated signal after channel estimation is congregated into a serial sequence, which is then demodulated and decoded by the corresponding methods in the transmitter. At this point, the output of UWA-OFDM system model is obtained as the final binary data sequence.

B. CHANNEL ESTIMATION

The aim of channel estimation is to estimate channel parameters from the received signal. As discussed in (6), each subcarrier component of the received signal can be expressed as the product of the transmitted signal and channel frequency response at the subcarrier as long as no inter-carrier interference (ICI) occurs. Thus, the transmitted signal can be recovered by estimating the channel response at each subcarrier. In general, channel estimation is executed with the help of pilot symbols, which are known to both transmitter and receiver. As shown in Fig. 2, the pilot symbols can be inserted into the frequency or time direction in OFDM frames, namely comb-type and block-type [59], respectively. After obtaining the state estimation at the pilot symbols, the channel responses of all subcarriers between pilot symbols can be estimated by employing various interpolation methods, such as linear interpolation, second-order interpolation, spline cubic interpolation [60].

LS algorithm is the most typical representative of the traditional channel estimation method, essentially to solve

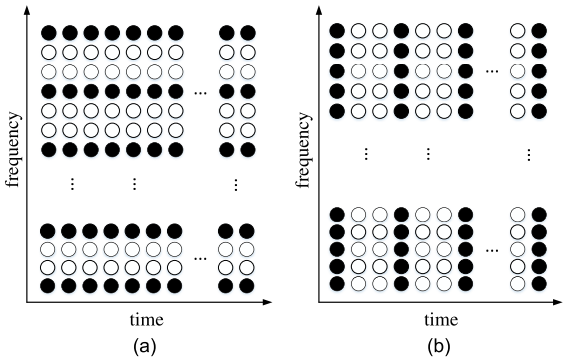

FIGURE 2. Two different types of pilot structures for UWA-OFDM systems. (a) Comb-type. (b) block-type. The solid circles indicate pilot symbols and the hollow circles indicate data symbols.

a problem of extreme value. Assuming the estimated channel impulse response is $\hat{\mathbf{H}}$, LS algorithm gives the solution to channel estimation for UWA-OFDM systems as follows [61]:

$$\hat{\mathbf{H}}_{LS} = (\mathbf{X}^H\mathbf{X})^{-1}\mathbf{X}^H\mathbf{Y} = \mathbf{X}^{-1}\mathbf{Y} \tag{7}$$

where the superscript $(\cdot)^H$ stands for the Hermitian transpose. It denotes that LS channel estimator is directly obtained by minimizing the square distance between the received symbols Y and the transmitted symbols X. Therefore, it is widely used for channel estimation due to its simplicity and without channel statistics required. However, it neglects the noise interference in the calculation process, resulting poor performance in complex UWA communication environment.

To overcome the noise-sensitive defects of LS algorithm, MMSE algorithm is calculated based on minimizing the mean square error (MSE) of the actual channel and its estimation. Combined with the LS channel estimation result $\hat{\mathbf{H}}_{LS}$ in (7), the MMSE estimator can be achieved as follows [61] :

$$\hat{\mathbf{H}}_{MMSE} = \mathbf{R}_{\mathbf{H}\tilde{\mathbf{H}}}(\mathbf{R}_{\mathbf{HH}} + \frac{\delta_n^2}{\delta_x^2}\mathbf{I})^{-1}\hat{\mathbf{H}}_{LS} \tag{8}$$

where $\mathbf{R}_{\mathbf{HH}} = E\left\{\mathbf{H}\mathbf{H}^H\right\}$ refers to the autocorrelation matrix of channel response in frequency domain, and $\mathbf{R}_{\mathbf{H}\tilde{\mathbf{H}}}$ denotes the cross-correlation matrix between the actual channel and temporary estimated channel. δ_n^2 and δ_x^2 are the variance of AWGN and transmitted signal, respectively. The influence of noise is taken into account by MMSE algorithm to improve the channel estimation accuracy. However, it is more complex than the LS algorithm because it requires some prior knowledge about the channel statistical properties, including the channel autocorrelation matrix and noise variance.

III. PROPOSED DNN-BASED METHODS

This section describes the architectures of our proposed DNN-based methods and the methodology of their usage for channel estimation in UWA-OFDM systems.

A. PRELIMINARY

In this subsection, we will begin by describing the simplest neural network with only a single neuron, as shown

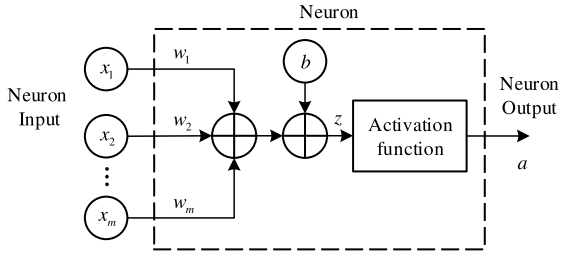

FIGURE 3. Inside structure of a neuron in the neural network. The neuron output is the calculation result of the inputs, weights, and a bias through an activation function.

in Fig. 3. The neuron is a computational unit related to the inputs $\{x_1, x_2, \ldots, x_m\}$, the weights $\{w_1, w_2, \ldots, w_m\}$ for corresponding inputs, and the bias b used to model the threshold. In this figure, the weighted computation z can be adopted as:

$$z = \sum_{i=1}^{m} w_i x_i + b \tag{9}$$

The output of the neuron, denoted by a, is the result of a linear or nonlinear transformation of variable z, as follows:

$$a = f(z) = f(\sum_{i=1}^{m} w_i x_i + b) \tag{10}$$

where $f(\cdot)$ is called the activation function. By introducing nonlinear factors into the neuron, the activation function translates the input signal to the output signal so that the neural network can approximate any nonlinear function arbitrarily.

Different activation functions and their variants have been proposed in various neural networks over the years [62]. Among them, the most commonly used activation functions, sigmoid, hyperbolic tangent (tanh), linear, and rectified linear unit (ReLU) functions, are respectively defined as:

$$f_1(z) = \frac{1}{1 + e^{-z}} \tag{11}$$

$$f_2(z) = tanh(z) = \frac{e^{z} - e^{-z}}{e^{z} + e^{-z}} \tag{12}$$

$$f_3(z) = cz + d \tag{13}$$

$$f_4(z) = \max(0, z) = \begin{cases} 0, & z \leq 0 \\ z, & z > 0 \end{cases} \tag{14}$$

Fig. 4 plots these four activation functions. Note that the sigmoid function squashes the real numbers to a different dynamic interval of [0, 1], while the hyperbolic tangent (tanh) function squashes to $[-1, 1]$. The ReLU function is a half-wave rectifier and it saturates at exactly 0 whenever the input z is less than 0. Unlike these three, the linear function does not condense the network input so that it can approximate to any real number as the network output.

B. NETWORK ARCHITECTURES

A neural network is usually comprised of numerous neurons as described in Fig. 3, which are fully interconnected to each other to form a grid. There is a weight factor between every two neurons in different adjacent layers and these weights are dynamically adjusted during the training process. This configuration makes the output of a neuron in the anterior layer can be the input of another neurons in the latter layer. A standard three-layer neural network is embedded in Fig. 1. The leftmost layer of the network is called the input layer, and the rightmost layer the output layer. The middle layer between the input layer and the output layer is called the hidden layers because their values are invisible in the training process.

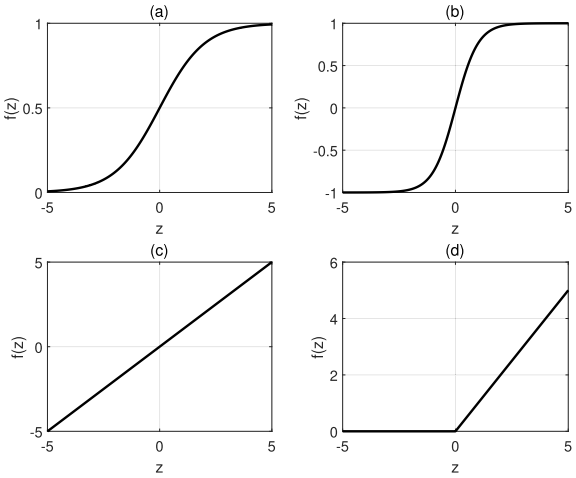

FIGURE 4. Commonly used activation functions in neural networks. (a) Sigmoid function. (b) hyperbolic tangent function (tanh). (c) linear function (here, $c = 1, d = 0$). (d) ReLU function.

It is well known that DNN inherits from the classical neural network but includes more hidden layers and more neurons. Its deep architecture promotes the model to yield better performance in very complex and highly nonlinear problems than the traditional methods. Hence in this paper, the DNN model, as illustrated in Fig. 5, is introduced to estimate the channel coefficients in UWA-OFDM systems since this approach is applicable in channel estimation problems for its outstanding learning, representation, and approximation ability.

C. MODEL TRAINING

In general, the deployment of DNN model contains two stages, the training process and the working process. Before implemented to estimate the channel parameters effectively in the working process, the network model must be trained by training symbols in the training process.

As can be seen in Fig. 5, assuming that L denotes the number of layers in our DNN model and $l \in [1, L]$ labels the l-th layer, thus layer 1 is the input layer and layer L is the output layer. We use w_{ij}^{l} to denote the weight for the connection from the j-th neuron in the $(l-1)$-th layer to the i-th neuron in the l-th layer. Similarly, b_i^l is used for the bias of the i-th neuron in the l-th layer, and a_i^l for the activation value of the i-th neuron in the l-th layer. With these notations,

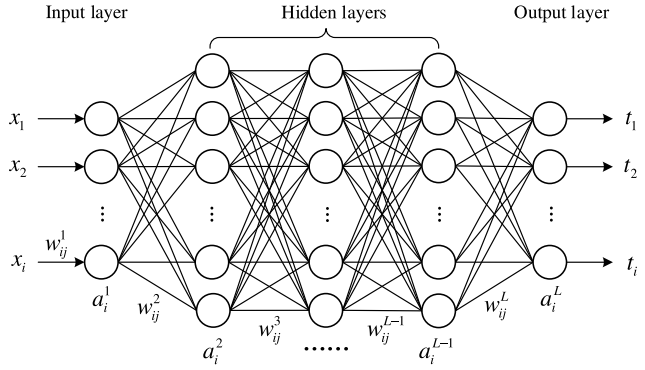

FIGURE 5. Typical architecture of deep neural network model. It consists of an input layer, multiple hidden layers, and an output layer. The neurons in the two adjacent layers are fully connected, whereas the neurons in each layer are not connected.

the computation of z_i^l and a_i^l are given by:

$$z_i^l = \sum_j w_{ij}^l a_j^{l-1} + b_i^l \tag{15}$$

$$a_i^l = f(z_i^l) = f(\sum_j w_{ij}^l a_j^{l-1} + b_i^l) \tag{16}$$

For simplicity in a matrix form, these expressions can be rewritten as:

$$\mathbf{z}^l = \mathbf{W}^l \mathbf{a}^{l-1} + \mathbf{b}^l \tag{17}$$

$$\mathbf{a}^l = f(\mathbf{z}^l) = f(\mathbf{W}^l \mathbf{a}^{l-1} + \mathbf{b}^l) \tag{18}$$

where $\mathbf{W}^l$ denotes the weight matrix between the $(l-1)$-th layer and l-th layer, $\mathbf{a}^{l-1}$ denotes the output vector of the $(l-1)$-th layer, and $\mathbf{b}^l$ is the bias vector for the l-th layer. Thus the neuron outputs in the L-th layer (i.e. the output layer) can be obtained as:

$$\mathbf{a}^L = f(\mathbf{z}^L) = f(\mathbf{W}^L \mathbf{a}^{L-1} + \mathbf{b}^L) \tag{19}$$

In the beginning of the training process, the weights and biases are initialized to small random values near zero for symmetry breaking. Then, the DNN is trained based on gradient descent using a given training set $\{(x_1, t_1), \ldots, (x_m, t_m)\}$ of m training symbols, where x_i and t_i $(i = 1, 2, \ldots, m)$ refer to the network inputs and target outputs. To measure the gap between the network outputs and the desired target outputs, the cost function is defined as follows:

$$\begin{aligned} E &= \frac{1}{2}\|\mathbf{a}^L - \mathbf{t}\|^2 \\ &= \frac{1}{2}\|f(\mathbf{W}^L \mathbf{a}^{L-1} + \mathbf{b}^L) - \mathbf{t}\|^2 \end{aligned} \tag{20}$$

where $\mathbf{t}$ is the matrix form of desired target outputs.

For the goal to minimize the cost function, the partial derivatives of weights and biases in the L-th layer can be computed respectively as follows:

$$\begin{aligned} \frac{\partial E}{\partial \mathbf{W}^L} &= \frac{\partial E}{\partial \mathbf{z}^L}\frac{\partial \mathbf{z}^L}{\partial \mathbf{W}^L} \\ &= (\mathbf{a}^L - \mathbf{t}) \odot f'(\mathbf{z}^L)(\mathbf{a}^{L-1})^T \end{aligned} \tag{21}$$

TABLE 1. Architectures of neural network models for channel estimation.

Layer	BPNN [31]		DNN-1[ours]		DNN-2[ours]	
	Nodes	$f(\cdot)$	Nodes	$f(\cdot)$	Nodes	$f(\cdot)$
Input	2	–	4	–	16	–
Hidden #1	10	tanh	32	tanh	64	tanh
Hidden #2	–	–	32	tanh	64	tanh
Hidden #3	–	–	32	tanh	64	tanh
Output	2	linear	4	linear	16	linear

$$\begin{aligned} \frac{\partial E}{\partial \mathbf{b}^L} &= \frac{\partial E}{\partial \mathbf{z}^L}\frac{\partial \mathbf{z}^L}{\partial \mathbf{b}^L} \\ &= (\mathbf{a}^L - \mathbf{t}) \odot f'(\mathbf{z}^L) \end{aligned} \tag{22}$$

where $\odot$ denotes the Hadamard product. We define an error term $\boldsymbol{\delta}^L$ for neurons in the output layer as:

$$\boldsymbol{\delta}^L = \frac{\partial E}{\partial \mathbf{z}^L} = (\mathbf{a}^L - \mathbf{t}) \odot f'(\mathbf{z}^L) \tag{23}$$

thus $\boldsymbol{\delta}^l$ in the l-th layer can be derived using the method of mathematical induction [63]:

$$\begin{aligned} \boldsymbol{\delta}^l &= \frac{\partial E}{\partial \mathbf{z}^l} = \boldsymbol{\delta}^{l+1}\frac{\partial \mathbf{z}^{l+1}}{\partial \mathbf{z}^l} \\ &= (\mathbf{W}^{l+1})^T \boldsymbol{\delta}^{l+1} \odot f'(\mathbf{z}^l) \end{aligned} \tag{24}$$

Once $\boldsymbol{\delta}^l$ is calculated in an iterative process of gradient descent, the weights and biases in the l-th layer will be updated as follows:

$$\mathbf{W}^{l*} = \mathbf{W}^l - \eta\frac{\partial E}{\partial \mathbf{W}^l} = \mathbf{W}^l - \eta\boldsymbol{\delta}^l(\mathbf{a}^{l-1})^T \tag{25}$$

$$\mathbf{b}^{l*} = \mathbf{b}^l - \eta\frac{\partial E}{\partial \mathbf{b}^l} = \mathbf{b}^l - \eta\boldsymbol{\delta}^l \tag{26}$$

where $\mathbf{W}^{l*}$ and $\mathbf{b}^{l*}$ correspond to the weights and biases of the next iteration. η refers to the learning rate between 0 and 1 that is used to determine the change in each update and impacts the convergence speed of model training.

As stated before, the training process of DNN model can be summed up as the forward propagation of the training symbols and the back propagation of the learning error, as presented in Fig. 6. Originally, the training input data are dealt by the neurons in hidden layers and then are transmitted to the output layer. If the results of the output layer do not match the desired ones, the learning errors between the network outputs and target outputs will be backtracked from the output layer to hidden layers. Meanwhile, the weights and biases in the neurons will be modified according to the learning errors, as described in (25) and (26), respectively. The training process will be repeated until the stopping criteria are reached, such as a given number of iterations have been completed, or a chosen goal of the learning error has been satisfied, etc.

In this paper, two DNN models, labeled by DNN-1 and DNN-2, are proposed for channel estimation with five layers, consisting of an input layer, three hidden layers and an output layer. As presented in Table. 1, the numbers of

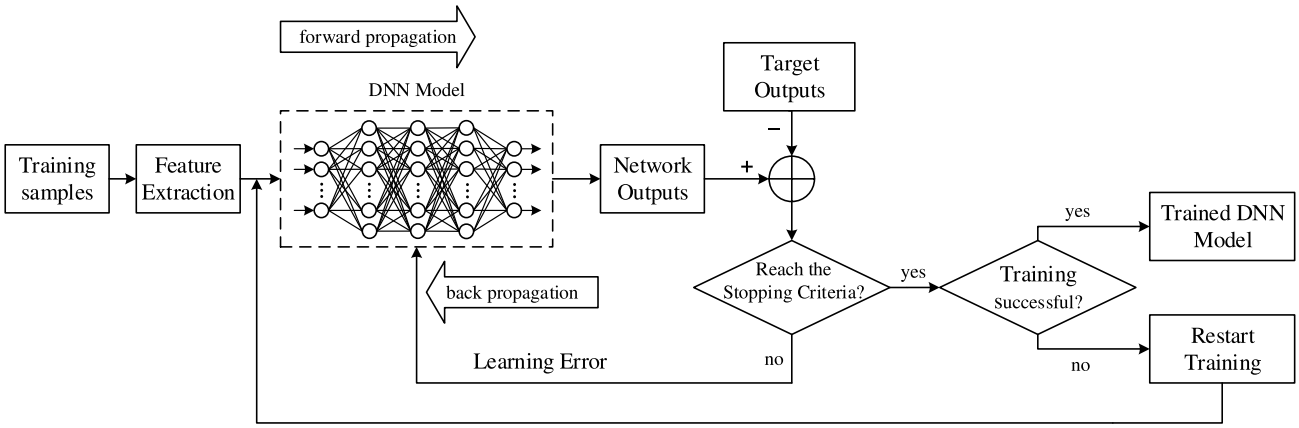

FIGURE 6. Training process of the proposed DNN models. The objective of training a DNN is to find the optimal parameters of weights and biases to minimise the error between the network outputs and the target outputs.

TABLE 2. Simulation parameters of the UWA-OFDM system.

Parameter	Value
Number of subcarriers	1024
FFT size	1024
Type of modulation	16, 32, 64QAM
Type of pilot insertion	Comb
Type of guard interval	Cyclic prefix
Length of guard interval	256
Channel model	UWA multipath channels
Noise model	Additive White Gaussian Noise

TABLE 3. Training parameters of neural network models.

Parameter	Value
Training function	Levenberg-Marquardt [26]
Maximum number of epochs	1000
Performance goal of training	1×10^{-5}
Minimum performance gradient	1×10^{-7}
Learning rate	0.05
Maximum validation failures	6

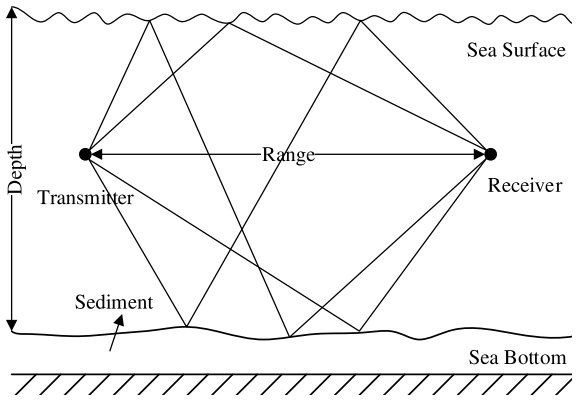

FIGURE 7. BELLHOP ray model of a shallow UWA multipath channel. It takes into account environmental factors including the variation of sound speed at depths, shapes of sea surface and bottom, boundary reflection and scattering, and geometry of the transmitter and receiver.

neurons in each layer are 4, 32, 32, 32, 4 in DNN-1 and 16, 64, 64, 64, 16 in DNN-2, respectively. These parameters of designed layers and neurons are obtained with iterative simulations. To adopt the UWA-OFDM signal to neural network, the complex signal is separated into real and imaginary parts, since neural network allows only the real format whereas the UWA-OFDM signal is in complex format. In our proposed channel estimator, the DNN models are firstly trained before deployment with the training received pilot symbols and the correct channel impulse responses in the training process. Every two pilot symbols and every eight pilot symbols are grouped into the models of DNN-1 and DNN-2 respectively, then the corresponding outputs of each DNN model are gathered together for the final outputs. Hyperbolic tangent function in (12) is chosen as the activation function in hidden layers and linear function in (13) is chosen in output layer, for both of these network models. Besides, 1,318,400 training samples, randomly divided into 70% as training set, 15% as test set, and 15% as validation set, are utilized to train the each considered type of neural network. Finally, in the working process, the current received pilot symbols are fed into the trained DNN models and the outputs of the networks will be the estimated channel impulse responses. The detailed procedure of DNN-based channel estimation is exhibited in Algorithm 1.

IV. EXPERIMENTS AND ANALYSIS

A. EXPERIMENTAL SETUP

To demonstrate the performance of our proposed DNN models for channel estimation, experiments have been carried out to compare with the conventional LS algorithm [13], MMSE algorithm [13] and BPNN [30] in terms of BER and NMSE versus SNR criteria. The parameters of the UWA-OFDM system and neural network training used in our simulations are given in Table. 2 and Table. 3, respectively.

Additionally, to increase the reliability and accuracy of our experiments, we utilize the BELLHOP ray

Algorithm 1 DNN-Based Channel Estimation Algorithm

%Training process
Initialize the weights $\mathbf{W}$ and biases $\mathbf{b}$ of the hidden layers and the output layer randomly. Configure the training parameters of DNN models with reasonable values, including the maximum number of epochs M_1, the performance goal ε, the minimum performance gradient ξ, the learning rate η, and the maximum validation failures M_2.
Input the training samples $\{(x_1, t_1), \ldots, (x_m, t_m)\}$, comprising of the training received pilot symbols x_i $(i = 1, 2, \ldots, m)$ and the correct channel impulse responses t_i $(i = 1, 2, \ldots, m)$.
repeat
    Calculate the network outputs of the output layer $\mathbf{a}^L$ according to (19).
    Calculate the value of the cost function E according to (20).
    Calculate the partial derivatives of weights and biases according to (21) and (22), respectively.
    Update the weights and biases with the learning rate η in an iterative process of gradient descent according to (25) and (26), respectively.
until {(iteration number $\geq M_1$) $\|$ (training performance $\leq \varepsilon$) $\|$ (performance gradient $\leq \xi$) $\|$ (validation failure number $\geq M_2$)}
if (a good training result is generated)
    Return the trained DNN model with optimal weights and biases as a complete black box for deployment.
else
    Restart the training process.
end if
%Working process
Feed the set of current received pilot symbols separated into real and imaginary parts as inputs to the trained DNN model.
Return the set of estimated channel impulse responses as outputs by collecting the real and imaginary parts together for channel estimation in UWA-OFDM systems.
Recover the transmitted signal with the estimated channel impulse responses and the received signal according to (6) in a noise environment.

model [6], [64], [65] to simulate the UWA communication environment in this paper. As illustrated in Fig. 7, the BELLHOP ray model is used to predict acoustic wave propagation in water columns with consideration of sound speed profile (SSP), boundaries of sea surface and sea bottom, reflection and scattering in boundaries, and geometry of the transmitter and receiver. The depth of water column is 100 m and the range between transmitter and receiver is approximately 1000 m. As expressed to be a function of temperature, salinity and depth, the sound speed increases from 1527 m/s at the surface of the water column to 1530 m/s at the bottom. In the sediment layer, the sound speed is 1650 m/s and the attenuation coefficient is 0.8 dB/λ. The density of water is 1.0 g/cm^3 and that of the sediment layer is 1.9 g/cm^3. Based on the schematic diagram of BELLHOP ray model in Fig. 7, two different UWA multipath channels with three taps and seven taps are modeled to investigate the performance of UWA-OFDM systems, labeled by channel-I and channel-II, respectively.

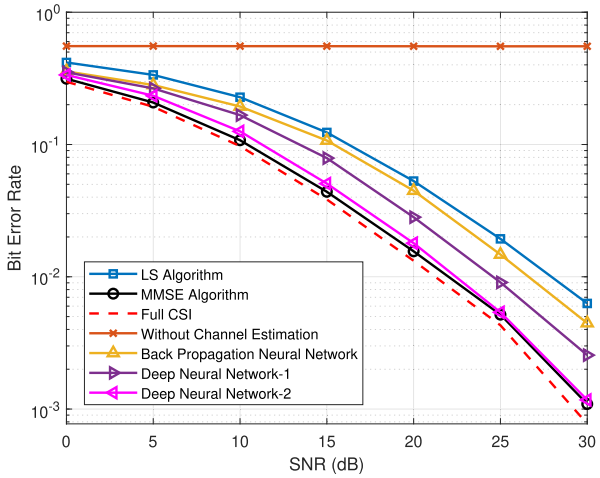

FIGURE 8. Comparison of BER performance over channel-I with 16QAM.

B. ESTIMATION PERFORMANCE ON BER AND NMSE

Fig. 8 and 9 present the BER performance of channel estimators based on various methods in UWA-OFDM systems over channel-I and channel-II, respectively. These estimation methods include LS, MMSE, BPNN, and the proposed DNN-1 and DNN-2. Moreover, the cases with full CSI and without channel estimation are also compared for performance analysis. The scheme of 16QAM is utilized to modulate the transmitted signal in this simulation.

According to the results in Fig. 8 and 9 over each channel, the BER values of all these methods gradually decreases as the SNR increases except the case without channel estimation, in which the BER performance has hardly improved with the increasing SNR from 0 dB to 30 dB. For both channels, LS algorithm performs the worst among the considered estimators. On the contrary, MMSE algorithm yields the best performance of BER at each SNR value, displaying the closest curve to the optimal case with full CSI. Our proposed two estimators based on DNN show better performance than LS algorithm and BPNN estimator not only for channel-I but also for channel-II. It is also clearly seen from the figures that, the DNN-2 estimator with more neurons ensures better BER result than DNN-1 estimator over both channels. As the increased SNR values, the performance of DNN-2 is getting closer to MMSE algorithm and the case with full CSI. The reason lies in the fact that the more neurons in the same number of layers can improve the learning accuracy

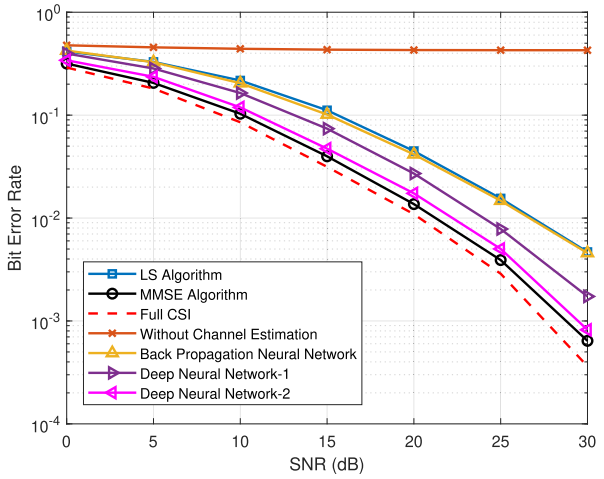

FIGURE 9. Comparison of BER performance over channel-II with 16QAM.

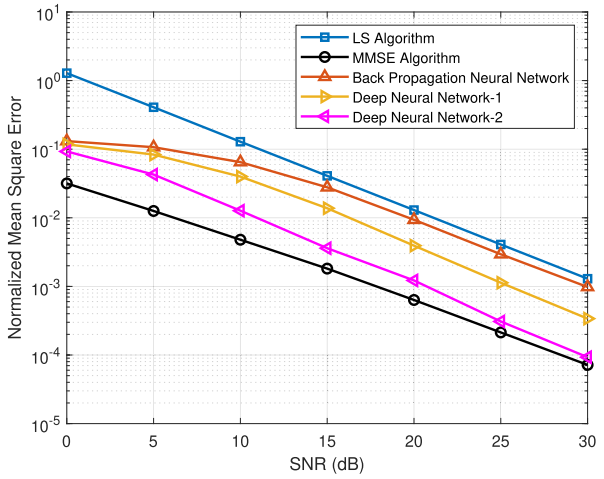

FIGURE 10. Comparison of NMSE performance over channel-I with 16QAM.

of neural network effectively for channel estimation. For instance, at SNR value of 25 dB in Fig. 8, the BER of DNN-2 estimator is approximately 5.4×10^{-3} almost the same as MMSE algorithm, whereas the BER of DNN-1 estimator is 9.1×10^{-3}, BPNN estimator is 1.5×10^{-2}, and LS algorithm is only 1.9×10^{-2}. Furthermore, in Fig. 10, DNN-2 estimator requires 1.5 dB less SNR than DNN-1 estimator and 4.3 dB less SNR than BPNN at BER value of 10^{-2}, respectively.

In this paper, NMSE is used as a measurement indicator to evaluate the estimation performance for SNR values in a certain interval. The expression of NMSE is defined as follows [10]:

$$NMSE = \sum_{k=1}^{N} \frac{\|\mathbf{H_{real}} - \mathbf{H_{est}}\|^2}{\|\mathbf{H_{real}}\|^2} \tag{27}$$

where $\mathbf{H_{real}}$ is the real channel frequency response and $\mathbf{H_{est}}$ is the estimated channel frequency response.

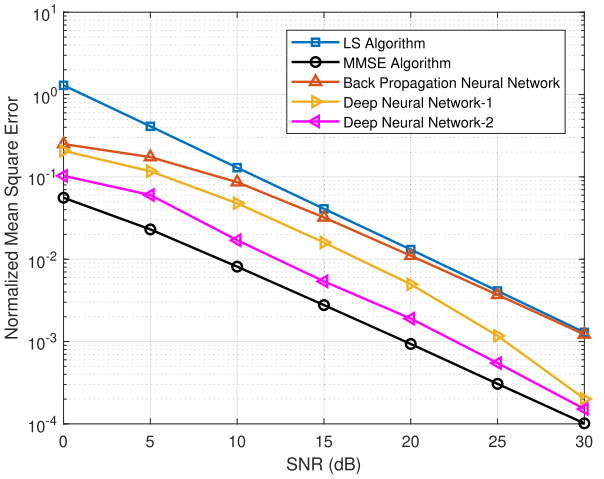

FIGURE 11. Comparison of NMSE performance over channel-II with 16QAM.

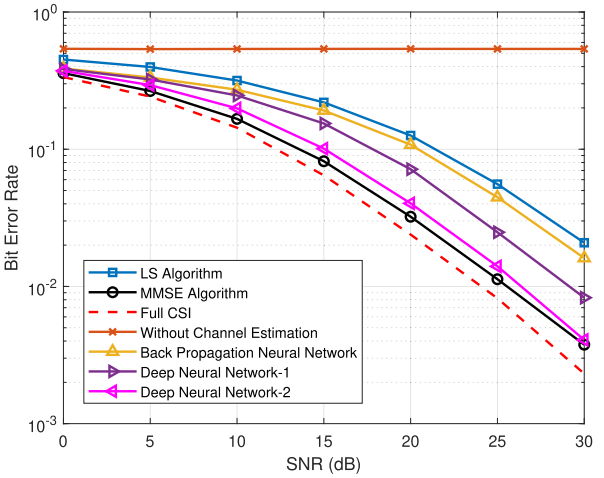

FIGURE 12. Comparison of BER performance over channel-I with 32QAM.

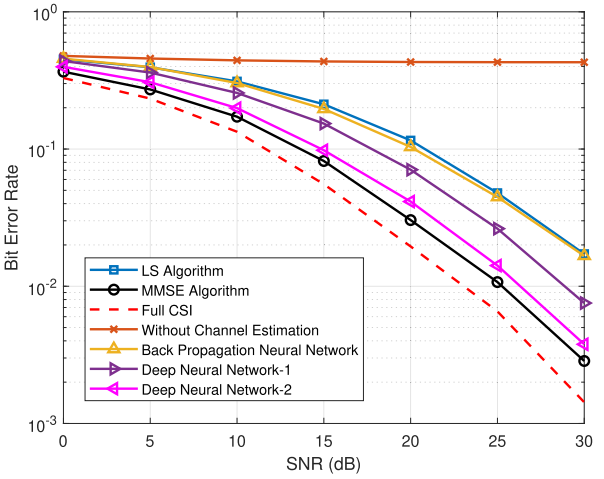

FIGURE 13. Comparison of BER performance over channel-II with 32QAM.

In Fig. 10 and 11, the NMSE performance of LS, MMSE, BPNN algorithms are compared with our proposed DNN-based estimators for UWA-OFDM systems over two

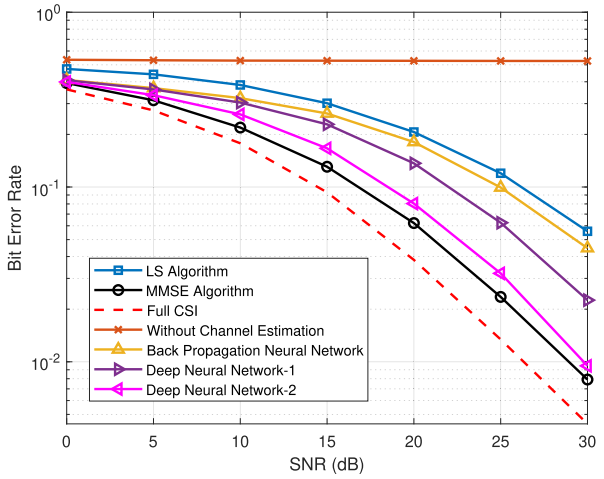

FIGURE 14. Comparison of BER performance over channel-I with 64QAM.

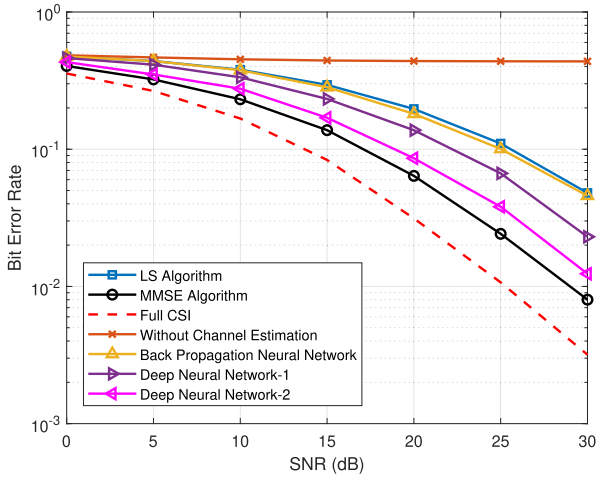

FIGURE 15. Comparison of BER performance over channel-II with 64QAM.

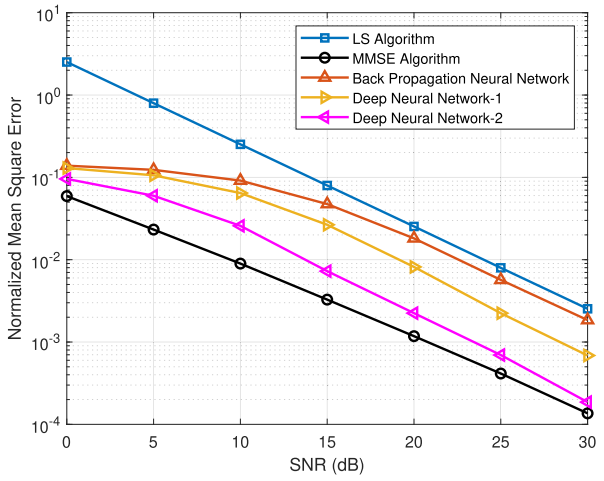

FIGURE 16. Comparison of NMSE performance over channel-I with 32QAM.

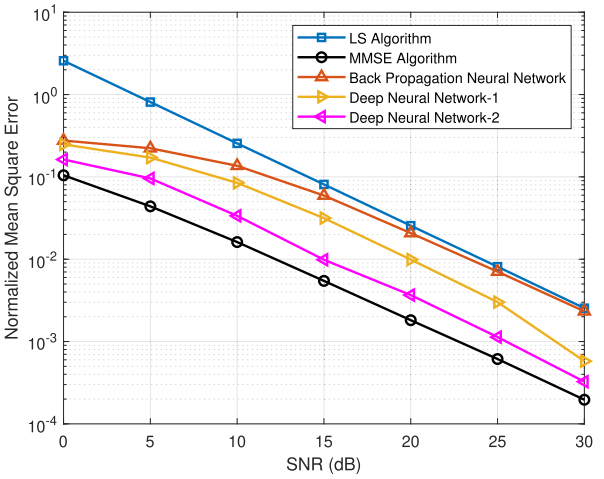

FIGURE 17. Comparison of NMSE performance over channel-II with 32QAM.

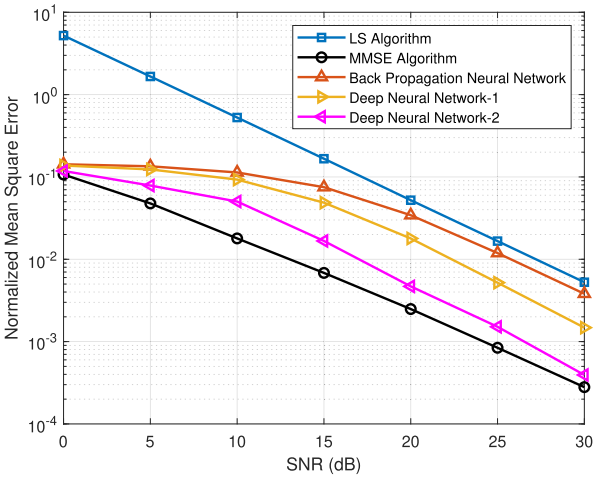

FIGURE 18. Comparison of NMSE performance over channel-I with 64QAM.

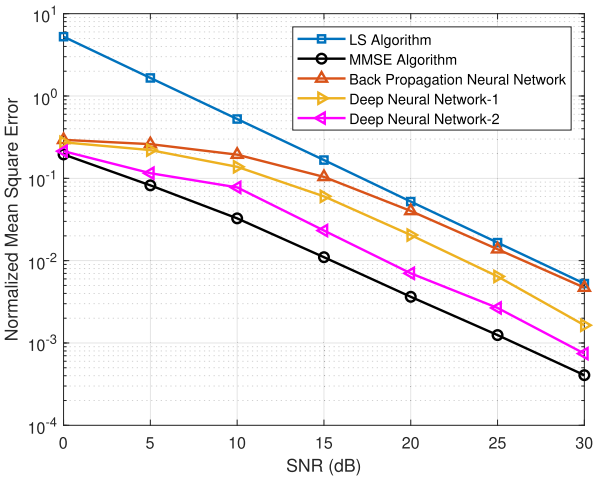

FIGURE 19. Comparison of NMSE performance over channel-II with 64QAM.

channels, respectively. As it can be observed from the figures, LS algorithm yields the worst performance while MMSE algorithm yields the best performance over both channels among the all considered methods. Estimation errors of the neural network based methods consisting of BPNN, DNN-1, and DNN-2 are between LS algorithm and MMSE

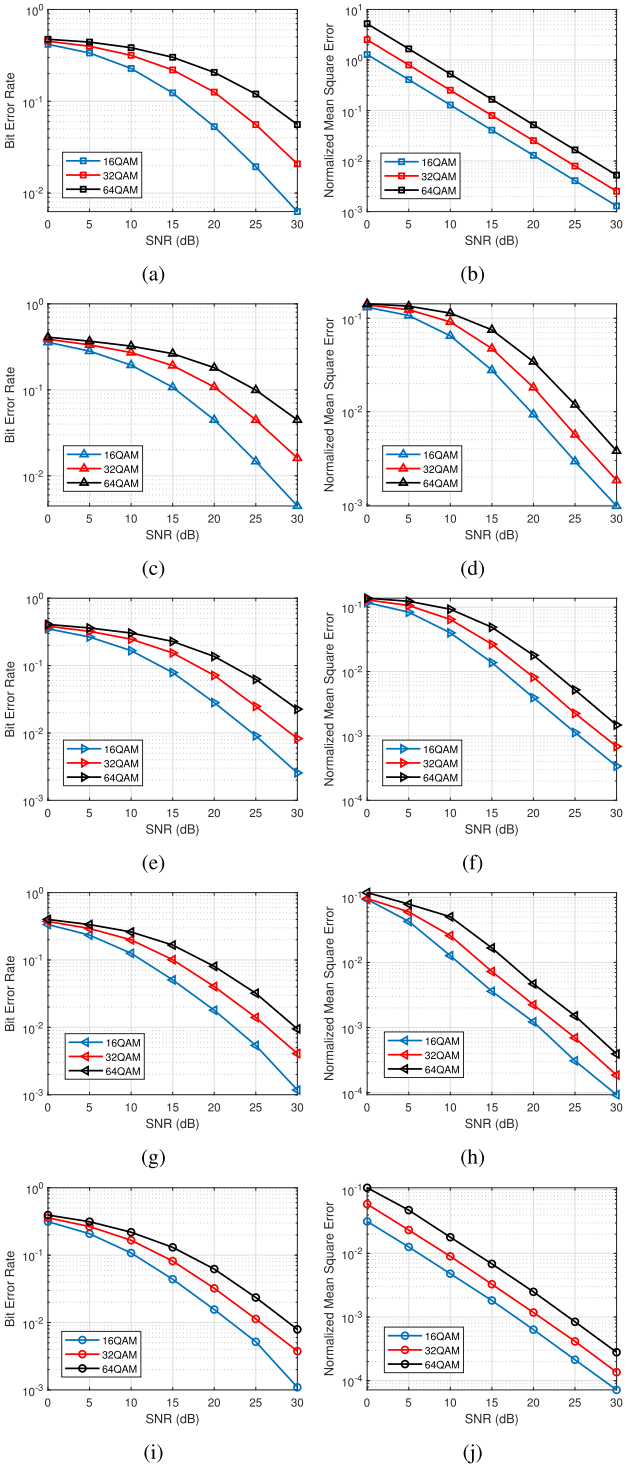

FIGURE 20. Comparison of BER and NMSE performance over channel-I for channel estimation in UWA-OFDM systems with various methods, each of which is modulated with 16QAM, 32QAM, and 64QAM, respectively. (a) BER for LS. (b) NMSE for LS. (c) BER for BPNN. (d) NMSE for BPNN. (e) BER for DNN-1. (f) NMSE for DNN-1. (g) BER for DNN-2. (h) NMSE for DNN-2. (i) BER for MMSE. (j) NMSE for MMSE.

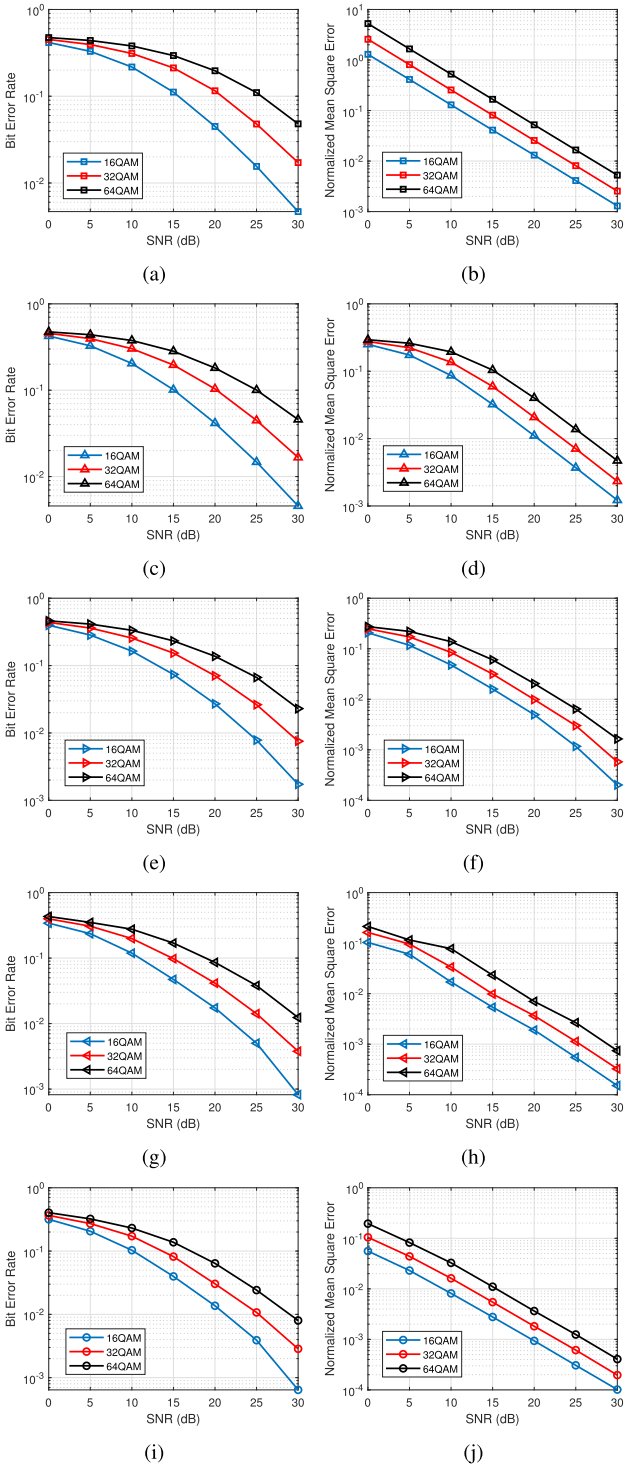

FIGURE 21. Comparison of BER and NMSE performance over channel-II for channel estimation in UWA-OFDM systems with various methods, each of which is modulated with 16QAM, 32QAM, and 64QAM, respectively. (a) BER for LS. (b) NMSE for LS. (c) BER for BPNN. (d) NMSE for BPNN. (e) BER for DNN-1. (f) NMSE for DNN-1. (g) BER for DNN-2. (h) NMSE for DNN-2. (i) BER for MMSE. (j) NMSE for MMSE.

algorithm for each SNR values. Among these three methods, DNN-2 estimator presents better performance than DNN-1 and BPNN, with being the closest curve to MMSE algorithm. For example, in Fig. 10, at the SNR value of 25 dB over channel-I, the NMSE of LS, BPNN, DNN-1, DNN-2, and MMSE are approximately 4.1×10^{-3}, 2.9×10^{-3}, 1.1×10^{-3},

TABLE 4. BER performance with different modulation schemes for the example in Fig. 22 and 23.

Method	Channel-I			Channel-II		
	64QAM	32QAM	16QAM	64QAM	32QAM	16QAM
LS [13]	0.2226	0.1346	0.0526	0.2104	0.1237	0.0460
BPNN [30]	0.1960	0.1170	0.0458	0.2005	0.1167	0.0453
DNN-1 [ours]	0.1657	0.0887	0.0323	0.1740	0.0909	0.0342
DNN-2 [ours]	0.1317	0.0573	0.0224	0.1401	0.0616	0.0238
MMSE [13]	0.0680	0.0335	0.0158	0.0716	0.0324	0.0144

TABLE 5. NMSE performance with different modulation schemes for the example in Fig. 22 and 23.

Method	Channel-I			Channel-II		
	64QAM	32QAM	16QAM	64QAM	32QAM	16QAM
LS [13]	0.1081	0.0557	0.0338	0.1058	0.0563	0.0349
BPNN [30]	0.0797	0.0426	0.0263	0.0928	0.0498	0.0326
DNN-1 [ours]	0.0522	0.0249	0.0141	0.0687	0.0332	0.0220
DNN-2 [ours]	0.0279	0.0095	0.0058	0.0392	0.0182	0.0109
MMSE [13]	0.0047	0.0026	0.0017	0.0072	0.0040	0.0025

3.1×10^{-4}, and 2.1×10^{-4}, respectively. Moreover, according to Fig. 11, the proposed DNN estimators have almost 10^{-1} advantage of NMSE performance than BPNN and LS at SNR value of 30 dB.

On the basis of observing the performance over different channels, various modulation schemes is also operated to further ascertain the robustness of our proposed DNN methods for channel estimation in UWA-OFDM systems. The BER performance of DNN-1, DNN-2 as well as the conventional LS, MMSE and BPNN algorithms in the modulation schemes of 32QAM and 64QAM are presented in Fig. 12, 14 over channel-I and in Fig. 13, 15 over channel-II, respectively. Meanwhile, Fig. 16, 17, 18, and 19 depict the NMSE performance of the considered methods in the corresponding conditions. According to the results, our proposed DNN-1 and DNN-2 estimators provide estimation performance superior to the LS, BPNN estimators but inferior to the MMSE estimator at each SNR values, for both the BER and NMSE curves. They are consistent with the case of 16QAM in Fig. 8, 9, 10, and 11. These analyses demonstrate our proposed DNN methods are robust and valid in different conditions for channel estimation.

Furthermore, it is noteworthy that although the MMSE estimator outperforms the proposed DNN estimators in the performance of BER and NMSE in above experiments, this technology requires prior statistics information about channel autocorrelation matrix and noise variance in UWA-OFDM systems. It is generally not feasible to obtain the prior information in real transmission scenarios. Therefore, the superiority of our proposed DNN estimators to the MMSE algorithm can be revealed with the fact that DNN estimators do not need any statistical knowledge for channel estimation and facilitate to implement in practical applications.

C. IMPACT OF MODULATION SCHEMES

To verify the influence of different modulation schemes on these channel estimation methods more clearly, the BER and NMSE performance of the considered LS, BPNN, DNN-1, DNN-2, and MMSE methods with 16QAM, 32QAM and 64QAM for UWA-OFDM systems are illustrated in Fig. 20 over channel-I and in Fig. 21 over channel-II, respectively.

As each subfigure shown in Fig. 20 and 21 from (a) to (j), when over the same channel-I or channel-II, it is noticeable that for these five methods, the values of BER and NMSE with the same modulation scheme of 16QAM, 32QAM, and 64QAM are decreasing as the SNR increases from 0 dB to 30 dB. It owes to the fact that the noise variance in UWA multipath channels, which is determined by the noise power, is also decreasing as the SNR increases. Meanwhile, in comparison of our proposed DNN-1 and DNN-2 as well as LS, BPNN, and MMSE methods with three modulations, both the BER and NMSE of 16QAM for each method outperform against 32QAM and 64QAM for each value of SNR, whereas 32QAM performs better than 64QAM. For example, if the attention is paid to the BER performance of DNN-2 in Fig. 20(g) at the SNR value of 30 dB, the BER with 16QAM is approximately 1.2×10^{-3} whereas the values with 32QAM and 64QAM are 4.1×10^{-3} and 9.5×10^{-3} respectively. Moreover, DNN-2 requires 23.2 dB, 27.0 dB, and 29.9 dB of SNR for 16QAM, 32QAM, and 64QAM respectively to achieve the BER performance of 10^{-2}. It means DNN-2 with 16QAM can save 3.8 dB and 6.7 dB compared with 32QAM and 64QAM in this case. That is because the increasing modulation order improves the requirement for the accuracy of neural network learning, such that a channel estimator with higher modulation order encounters more difficulty in classifying the received signal to different constellation points

FIGURE 22. An example of image transmission with Lena (the pixel size is 256 × 256) is applied to visualize the impact of different modulation schemes for various methods in the UWA-OFDM system over channel-I, where the value of SNR is set to 20 dB. The first column shows the original transmitted images. The second to sixth columns show the reconstructed results from LS, BPNN, the proposed DNN-1, DNN-2, and MMSE methods. The original image data are modulated with 64QAM, 32QAM, and 16QAM in these three rows, respectively. (a) original. (b) LS(64QAM). (c) BPNN(64QAM). (d) DNN-1(64QAM). (e) DNN-2(64QAM). (f) MMSE(64QAM). (g) original. (h) LS(32QAM). (i) BPNN(32QAM). (j) DNN-1(32QAM). (k) DNN-2(32QAM). (l) MMSE(32QAM). (m) original. (n) LS(16QAM). (o) BPNN(16QAM). (p) DNN-1(16QAM). (q) DNN-2(16QAM). (r) MMSE(16QAM).

accurately, compared with lower modulation order. In fact, these results in line with expectations also prove the reasonability and validity of our proposed DNN methods.

Further to visualize the impact of different modulation schemes, Fig. 22 and 23 present an example of image transmission over channel-I and channel-II. An image of Lena with pixel size of 256 × 256 is utilized as the original transmitted data in this experiment. In both channels, the values of SNR are set as 20 dB to imitate the similar noise environment. We compare the reconstructed results from the proposed DNN-1, DNN-2 methods with LS, BPNN, and MMSE algorithms in the modulations of 64QAM, 32QAM, and 16QAM respectively.

For each row in Fig. 22 and 23, it can be seen that our proposals provide competitive performance over the other methods. Particularly for each column, the quality of restored images with 16QAM is obviously better than the ones with 32QAM and 64QAM for each method in both channels, where the 32QAM is next and the 64QAM is the worst as shown. More accurate results of quantitative evaluation containing the BER and NMSE are stated in Table. 4 and Table. 5, respectively. For instance, when the original image is transmitted in channel-I, the BER performance of DNN-2 suffers as low as 0.0224 from 16QAM whereas the value is as 2.5 times higher as 0.0573 from 32QAM and as 5.8 times higher as 0.1317 from 64QAM. Additionally, in the same scenario, the NMSE performance of DNN-2 achieves as low as 0.0058 from 16QAM, yet the value is as 1.6 times higher as 0.0095 from 32QAM and as 4.8 times higher as 0.0279 from 64QAM. These statistic data clearly reveal the impact of different modulation schemes for the proposed DNN-1, DNN-2 as well as LS, BPNN, and MMSE methods.

D. COMPARISON OF REAL-TIME PERFORMANCE

According to the example of Lena, the comparison results of real-time performance for neural network models with different architectures are indicated in Table. 6. The number of parameters is composed of the weights and bias terms in networks which occupy the most of storage resources, and the runtime refers to the average operational time using the trained network models to predict data in the working process. The simulations are performed in MATLAB R2018a using an Intel Core i7 CPU at 3.60 GHz and 8 GB of memory storage.

It is clear that the more neurons and parameters a model has, the longer the running time and the more storage resources it takes. As shown in Table. 6, the BPNN model including 14 neurons and 52 parameters costs the least runtime with 98.8 ms only. Our proposed DNN-2 model including 224 neurons and 10,448 parameters takes even 449.8 ms for operations in the working process, which is about twice as long as the DNN-1 model including 104 neurons and

FIGURE 23. An example of image transmission with Lena (the pixel size is 256 × 256) is applied to visualize the impact of different modulation schemes for various methods in the UWA-OFDM system over channel-II, where the value of SNR is also set to 20 dB. The first column shows the original transmitted images. The second to sixth columns show the reconstructed results from LS, BPNN, the proposed DNN-1, DNN-2, and MMSE methods. The original image data are modulated with 64QAM, 32QAM, and 16QAM in these three rows, respectively. (a) original. (b) LS(64QAM). (c) BPNN(64QAM). (d) DNN-1(64QAM). (e) DNN-2(64QAM). (f) MMSE(64QAM). (g) original. (h) LS(32QAM). (i) BPNN(32QAM). (j) DNN-1(32QAM). (k) DNN-2(32QAM). (l) MMSE(32QAM). (m) original. (n) LS(16QAM). (o) BPNN(16QAM). (p) DNN-1(16QAM). (q) DNN-2(16QAM). (r) MMSE(16QAM).

TABLE 6. Comparison of real-time performance for neural network models with different architectures.

Method	Layers	Neurons	Parameters	Runtime(ms)
BPNN [30]	3	14	52	98.8
DNN-1 [ours]	5	104	2,404	265.2
DNN-2 [ours]	5	224	10,448	449.8
Ye's [53]	6	604	47,848	–
Ye's [52]	5	1142	285,806	–
Zhang's [54]	5	3284	2,519,156	–

2,404 parameters with 265.2 ms since it contains about 4.3 times as many parameters as DNN-1. Correspondingly, it can be inferred that the DNN models in [52]–[54] will cost much more storage resources and running time than the DNN-2 model due to the larger number of network neurons and parameters. In particular, although DNN-1 is slightly inferior to DNN-2 in estimation performance of BER and NMSE as shown from Fig. 8 to 19, it can save about 77.0% of storage resources and 41.0% of running time in a certain precision range. If there is low latency requirement for channel estimation in UWA-OFDM systems, DNN-1 will be an option to consider because it makes a trade-off between real-time performance and estimation performance in practice.

V. CONCLUSIONS

In this paper, two types of DNN models termed DNN-1 and DNN-2 are specifically proposed for channel estimation in UWA-OFDM systems over multipath channels based on the BELLHOP ray model. Our proposed DNN models are trained with the received pilot symbols and the correct channel impulse responses in the training process, and the estimated channel impulse responses are offered by the outputs of the trained networks in the working process. Utilizing different modulation schemes of 16QAM, 32QAM, and 64QAM, the performance of the proposed methods is compared with LS, MMSE and BPNN methods with regards to BER and NMSE versus SNR values, respectively.

According to the experimental results, our proposed DNN methods outperform conventional LS and BPNN methods and yield close performance to MMSE algorithm in view of both BER and NMSE over the values of SNR from 0 dB to 30 dB. Although MMSE algorithm provides better performance than the proposed methods, it is complex as compared to other estimators and it involves prior statistics information about channel autocorrelation matrix and noise variance, which is generally not feasible to obtain in real communication scenarios. However, our proposed DNN methods do not require any prior statistical knowledge for channel estimation unlike the MMSE estimator. It demonstrates that the proposed

DNN methods have advantages in dealing with the problem of channel estimation in UWA-OFDM systems, due to the strong ability to analyze and learn the complicated characteristics of the UWA channels with serious distortions and interferences. Comparing with the impact of different modulation schemes, the proposed DNN models using 16QAM achieve better performance than those using 32QAM and 64QAM, as well as LS, BPNN, and MMSE methods. Furthermore, the DNN-1 model is superior to the DNN-2 model in storage resources and running time but slightly worse in estimation performance, so that it can be applicable for communication scenarios that prioritize the real-time performance in UWA-OFDM systems.

REFERENCES

[1] J. Preisig, "Acoustic propagation considerations for underwater acoustic communications network development," *ACM SIGMOBILE Mobile Comput. Commun. Rev.*, vol. 11, no. 4, pp. 2–10, Oct. 2007.

[2] M. Stojanovic and J. Preisig, "Underwater acoustic communication channels: Propagation models and statistical characterization," *IEEE Commun. Mag.*, vol. 47, no. 1, pp. 84–89, Jan. 2009.

[3] R. Diamant and L. Lampe, "Low probability of detection for underwater acoustic communication: A review," *IEEE Access*, vol. 6, pp. 19099–19112, 2018.

[4] G. Qiao, Z. Babar, L. Ma, S. Liu, and J. Wu, "MIMO-OFDM underwater acoustic communication systems—A review," *Phys. Commun.*, vol. 23, pp. 56–64, Jun. 2017.

[5] T. Lufen and X. Xu, *Digital Underwater Acoustic Communications*, 1st ed. New York, NY, USA: Academic, 2017.

[6] R. Jiang, S. Cao, C. Xue, and L. Tang, "Modeling and analyzing of underwater acoustic channels with curvilinear boundaries in shallow ocean," in *Proc. IEEE Int. Conf. Signal Process., Commun. Comput. (ICSPCC)*, Oct. 2017, pp. 1–6.

[7] P. C. Etter, *Underwater Acoustic Modeling and Simulation*. Boca Raton, FL, USA: CRC Press, 2018.

[8] R. Prasad, *OFDM for Wireless Communications Systems*. Norwood, MA, USA: Artech House, 2004.

[9] B. Li, S. Zhou, M. Stojanovic, L. Freitag, and P. Willett, "Multicarrier communication over underwater acoustic channels with nonuniform Doppler shifts," *IEEE J. Ocean. Eng.*, vol. 33, no. 2, pp. 198–209, Apr. 2008.

[10] P. Vimala and G. Yamuna, "Pilot design strategies for block sparse channel estimation in OFDM systems," *Indian J. Sci. Technol.*, vol. 10, no. 24, pp. 1–6, 2017.

[11] R. v. Nee and R. Prasad, *OFDM for Wireless Multimedia Communications*. Norwood, MA, USA: Artech House, 2000.

[12] Y. Liu, Z. Tan, H. Hu, L. J. Cimini, and G. Y. Li, "Channel estimation for OFDM," *IEEE Commun. Surveys Tuts.*, vol. 16, no. 4, pp. 1891–1908, 4th Quart., 2014.

[13] A. B. Singh and V. K. Gupta, "Performance evaluation of MMSE and LS channel estimation in OFDM system," *Int. J. Eng. Trends Technol.*, vol. 15, no. 1, pp. 39–43, 2014.

[14] M. B. Sutar and V. S. Patil, "LS and MMSE estimation with different fading channels for OFDM system," in *Proc. Int. Conf. Electron., Commun. Aerosp. Technol. (ICECA)*, vol. 1, Apr. 2017, pp. 740–745.

[15] W. Samek, S. Stanczak, and T. Wiegand. (2017). "The convergence of machine learning and communications." [Online]. Available: https://arxiv.org/abs/1708.08299

[16] M. Egmont Petersen, D. D. Ridder, and H. Handels, "Image processing with neural networks—A review," *Pattern Recognit.*, vol. 35, no. 10, pp. 2279–2301, 2002.

[17] A. Cochocki and R. Unbehauen, *Neural Networks for Optimization and Signal Processing*. Hoboken, NJ, USA: Wiley, 1992.

[18] A. Krizhevsky, I. Sutskever, and G. E. Hinton, "ImageNet classification with deep convolutional neural networks," in *Proc. Adv. Neural Inf. Process. Syst.*, 2012, pp. 1097–1105.

[19] S. Li, J. He, Y. Li, and M. U. Rafique, "Distributed recurrent neural networks for cooperative control of manipulators: A game-theoretic perspective," *IEEE Trans. Neural Netw. Learn. Syst.*, vol. 28, no. 2, pp. 415–426, Feb. 2017.

[20] Y. Li, S. Li, and B. Hannaford, "A model based recurrent neural network with randomness for efficient control with applications," *IEEE Trans. Ind. Informat.*, to be published. doi: 10.1109/TII.2018.2869588.

[21] Y. Li, S. Li, D. Caballero, M. Miyasaka, A. Lewis, and B. Hannaford, "Improving control precision and motion adaptiveness for surgical robot with recurrent neural network," in *Proc. IEEE/RSJ Int. Conf. Intell. Robots Syst. (IROS)*, Sep. 2017, pp. 3538–3543.

[22] Y. Li, S. Li, and B. Hannaford, "A novel recurrent neural network for improving redundant manipulator motion planning completeness," in *Proc. IEEE Int. Conf. Robot. Autom. (ICRA)*, May 2018, pp. 2956–2961.

[23] X. W. He, R. Z. Yang, J. Zhang, and Y. H. Zhang, "An OFDM channel estimation method with radial basis function neural network," *Appl. Mech. Mater.*, vol. 263, pp. 1142–1149, Dec. 2013.

[24] M. N. Seyman and N. Taspinar, "Radial basis function neural networks for channel estimation in MIMO-OFDM systems," *Arabian J. Sci. Eng.*, vol. 38, no. 8, pp. 2173–2178, 2013.

[25] C. S. Şimşir and N. Taşpınar, "Channel estimation using radial basis function neural network in OFDM-IDMA system," *Wireless Pers. Commun.*, vol. 85, no. 4, pp. 1883–1893, 2015.

[26] C. Çiflikli, A. T. Özşahin, and A. Ç. Yapici, "Artificial neural network channel estimation based on levenberg-marquardt for OFDM systems," *Wireless Pers. Commun.*, vol. 51, no. 2, pp. 221–229, 2009.

[27] S. J. Nawaz, S. Mohsin, and A. A. Ikaram, "Neural network based MIMO-OFDM channel equalizer using comb-type pilot arrangement," in *Proc. Int. Conf. Future Comput. Commun.*, 2009, pp. 36–41.

[28] M. N. Seyman and N. Taşpinar, "Channel estimation based on neural network with feedback for MIMO OFDM mobile communication systems," *Intell. Automat. Soft Comput.*, vol. 18, no. 3, pp. 307–316, 2012.

[29] E. Chen, R. Tao, and X. Zhao, "Channel equalization for OFDM system based on the BP neural network," in *Proc. 8th Int. Conf. Signal Process.*, vol. 3, 2006, pp. 2253–2256.

[30] N. Taşpinar and M. N. Seyman, "Back propagation neural network approach for channel estimation in OFDM system," in *Proc. IEEE Int. Conf. Wireless Commun., Netw. Inf. Secur. (WCNIS)*, Jun. 2010, pp. 265–268.

[31] C. H. Cheng, Y.-P. Cheng, Y.-H. Huang, and W.-C. Li, "Using back propagation neural network for channel estimation and compensation in OFDM systems," in *Proc. 7th Int. Conf. Complex, Intell., Softw. Intensive Syst. (CISIS)*, 2013, pp. 340–345.

[32] K. Hiray and K. V. Babu, "A neural network based channel estimation scheme for OFDM system," in *Proc. Int. Conf. Commun. Signal Process. (ICCSP)*, 2016, pp. 0438–0441.

[33] L. Zhang and X. Zhang, "MIMO channel estimation and equalization using three-layer neural networks with feedback," *Tsinghua Sci. Technol.*, vol. 12, no. 6, pp. 658–662, 2007.

[34] M. N. Seyman and N. Taşpinar, "Channel estimation based on neural network in space time block coded MIMO-OFDM system," *Digit. Signal Process.*, vol. 23, no. 1, pp. 275–280, 2013.

[35] C. S. Şimşir and N. Taşpinar, "Channel estimation using neural network in orthogonal frequency division multiplexing-interleave division multiple access (OFDM-IDMA) system," in *Proc. Telecommun. Symp.*, 2014, pp. 1–5.

[36] R. Choubey and V. Reddy, "Channel estimation in space time block coded MIMO-OFDM system: A review," *Int. J. Adv. Technol. Eng. Explor.*, vol. 5, no. 38, pp. 17–22, 2018.

[37] C. H. Cheng, Y. H. Huang, and H. C. Chen, "Channel estimation in OFDM systems using neural network technology combined with a genetic algorithm," *Soft Comput.*, vol. 20, no. 10, pp. 4139–4148, 2016.

[38] J. Schmidhuber, "Deep learning in neural networks: An overview," *Neural Netw.*, vol. 61, pp. 85–117, Jan. 2015.

[39] N. Akhtar and A. Mian, "Threat of adversarial attacks on deep learning in computer vision: A survey," *IEEE Access*, vol. 6, pp. 14410–14430, 2018.

[40] T. Young, D. Hazarika, S. Poria, and E. Cambria, "Recent trends in deep learning based natural language processing," *IEEE Comput. Intell. Mag.*, vol. 13, no. 3, pp. 55–75, Aug. 2018.

[41] Y. Zhang, W. Chan, and N. Jaitly, "Very deep convolutional networks for end-to-end speech recognition," in *Proc. IEEE Int. Conf. Acoust., Speech Signal Process. (ICASSP)*, Mar. 2017, pp. 4845–4849.

[42] X. Wang, L. Gao, and S. Mao, "BiLoc: Bi-modal deep learning for indoor localization with commodity 5GHz WiFi," *IEEE Access*, vol. 5, pp. 4209–4220, 2017.

[43] X. Wang, X. Wang, and S. Mao, "Deep convolutional neural networks for indoor localization with CSI images," *IEEE Trans. Netw. Sci. Eng.*, to be published. doi: 10.1109/TNSE.2018.2871165.

[44] C.-B. Ha and H.-K. Song, "Signal detection scheme based on adaptive ensemble deep learning model," *IEEE Access*, vol. 6, pp. 21342–21349, 2018.
[45] C. Luo, J. Ji, Q. Wang, X. Chen, and P. Li, "Channel state information prediction for 5G wireless communications: A deep learning approach," *IEEE Trans. Netw. Sci. Eng.*, to be published. doi: 10.1109/TNSE.2018.2848960.
[46] S. Peng *et al.*, "Modulation classification based on signal constellation diagrams and deep learning," *IEEE Trans. Neural Netw. Learn. Syst.*, to be published. doi: 10.1109/TNNLS.2018.2850703.
[47] C.-B. Ha, Y.-H. You, and H.-K. Song, "Machine learning model for adaptive modulation of multi-stream in MIMO-OFDM system," *IEEE Access*, vol. 7, pp. 5141–5152, 2018.
[48] M. Kim, W. Lee, and D.-H. Cho, "A novel PAPR reduction scheme for OFDM system based on deep learning," *IEEE Commun. Lett.*, vol. 22, no. 3, pp. 510–513, Mar. 2018.
[49] Q. Huang, C. Zhao, M. Jiang, X. Li, and J. Liang. (2018). "Cascadenet: A new deep learning architecture for OFDM detection." [Online]. Available: https://arxiv.org/abs/1812.00023
[50] E. Balevi and J. G. Andrews. (2018). "One-bit OFDM receivers via deep learning." [Online]. Available: https://arxiv.org/abs/1811.00971
[51] X. Gao, S. Jin, C.-K. Wen, and G. Y. Li, "ComNet: Combination of deep learning and expert knowledge in OFDM receivers," *IEEE Commun. Lett.*, vol. 22, no. 12, pp. 2627–2630, Dec. 2018.
[52] H. Ye, G. Y. Li, and B.-H. Juang, "Power of deep learning for channel estimation and signal detection in OFDM systems," *IEEE Wireless Commun. Lett.*, vol. 7, no. 1, pp. 114–117, Feb. 2018.
[53] H. Ye and G. Y. Li, "Initial results on deep learning for joint channel equalization and decoding," in *Proc. Veh. Technol. Conf.*, 2018, pp. 1–5.
[54] Y. Zhang, J. Li, Y. Zakharov, D. Sun, and J. Li, "Underwater acoustic OFDM communications using deep learning," 2018. [Online]. Available: https://eprints.soton.ac.uk/426097/1/FCAC_Deeplearning_OFDM_finally.pdf
[55] J. Dang, F. Qu, Z. Zhang, and L. Yang, "OFDM-IDMA communications over underwater acoustic channels," in *Proc. Military Commun. Conf. Milcom*, 2011, pp. 418–423.
[56] L. Liu *et al.*, "PN sequence based doppler and channel estimation for underwater acoustic OFDM communication," in *Proc. IEEE Int. Conf. Signal Process., Commun. Comput. (ICSPCC)*, Aug. 2016, pp. 1–6.
[57] Z. Wang, W. Han, and S. Liu, "An improved sparse underwater acoustic OFDM channel estimation method based on joint sparse model and exponential smoothing," in *Proc. ICPCC*, 2017, pp. 1–6.
[58] P. Chen, Y. Rong, S. Nordholm, Z. He, and A. J. Duncan, "Joint channel estimation and impulsive noise mitigation in underwater acoustic OFDM communication systems," *IEEE Trans. Wireless Commun.*, vol. 16, no. 9, pp. 6165–6178, Sep. 2017.
[59] S. Coleri, M. Ergen, A. Puri, and A. Bahai, "Channel estimation techniques based on pilot arrangement in OFDM systems," *IEEE Trans. Broadcast.*, vol. 48, no. 3, pp. 223–229, Sep. 2002.
[60] V. D. B. Janjaap, O. Edfors, M. Sandell, S. K. Wilson, and P. O. Borjesson, "On channel estimation in OFDM systems," in *Proc. Veh. Technol. Conf.*, 1995, pp. 815–819.
[61] S. C. Yong, J. Kim, W. Y. Yang, and C. G. Kang, *MIMO-OFDM Wireless Communications with MATLAB*. Hoboken, NJ, USA: Wiley, 2010.
[62] Y. H. Hu and J.-N. Hwang, "Introduction to neural networks for signal processing," in *Handbook of Neural Network Signal Processing*. Boca Raton, FL, USA: CRC Press, 2002, pp. 12–41.
[63] (2011). *Unsupervised Learning and Deep Learning Tutorial*. [Online]. Available: http://ufldl.stanford.edu/wiki/
[64] M. B. Porter and H. P. Bucker, "Gaussian beam tracing for computing ocean acoustic fields," *J. Acoust. Soc. Amer.*, vol. 82, no. 4, pp. 1349–1359, Oct. 1987.
[65] M. B. Porter, "The BELLHOP manual and user's guide: Preliminary draft," Heat, Light, and Sound Res., La Jolla, CA, USA, Tech. Rep., 2011 [Online]. Available: http://oalib.hlsresearch.com/Rays/HLS-2010–1.pdf

RONGKUN JIANG received the B.Eng. degree in electronic information engineering from the School of Information and Electronics, Beijing Institute of Technology, Beijing, China, in 2012, where he is currently pursuing the Ph.D. degree in electronic science and technology engineering. His current research interests include underwater acoustic communication, OFDM systems, compressed sensing, and channel estimation with applications of neural networks.

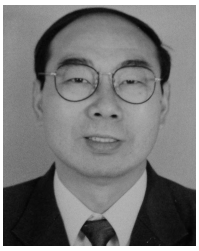

XUETIAN WANG received the B.Eng. and Ph.D. degrees in electronic engineering from the Beijing Institute of Technology, Beijing, China, in 1986 and 2002, respectively, where he is currently a Full Professor with the School of Information and Electronics. His current research interests include antenna theory and applications, millimeter-wave imaging, EMC, and terahertz radar.

SHAN CAO received the B.Eng. and Ph.D. degrees in microelectronics from Tsinghua University, China, in 2009 and 2015, respectively. She is currently an Assistant Professor with Shanghai University, China. Her research interests include design and implementation of wireless communication systems, design and implementation of signal processing systems, and integrated circuit design of neural networks.

JIAFEI ZHAO received the B.Eng. degree from the Chongqing University of Posts and Telecommunications, Chongqing, China, in 2013. She is currently pursuing the Ph.D. degree in electronic science and technology engineering with the School of Information and Electronics, Beijing Institute of Technology, Beijing. Her current research interests include clutter generation, system modeling, and neural networks.

XIAORAN LI received the B.Eng. degree in telecommunication engineering from the Beijing University of Posts and Telecommunications, Beijing, China, in 2011, and the M.E. and Ph.D. degrees in electronics science and technology from the Beijing Institute of Technology, Beijing, in 2013 and 2017, respectively. She was a Visiting Scholar with the Department of Electrical and Computer, Duke University, NC, USA, from 2015 to 2016. She is currently a Postdoctoral Research Fellow with the School of Information and Electronics, Beijing Institute of Technology. Her research interests include analog, radio frequency and millimeter-wave integrated circuits design, and circuits for biomedical applications.